This article was downloaded by: [Harbin Institute of Technology]
On: 28 December 2013, At: 18:47
Publisher: Taylor & Francis
Informa Ltd Registered in England and Wales Registered Number: 1072954 Registered office: Mortimer House, 37-41 Mortimer Street, London W1T 3JH, UK

Journal of Macromolecular Science, Part B: Physics
Publication details, including instructions for authors and subscription information:
http://www.tandfonline.com/loi/lmsb20

Aromatic Polyimide/MWCNT Hybrid Nanocomposites: Structure, Dynamics, and Properties

Baode Zhang [a], Vladimir Bershtein [b], Tatiana Sukhanova [c], Wanchen Zang [d], Chunhai Chen [d], Larisa Egorova [b], Iosif Gofman [c], Galina Gubanova [c], Anatoly Volkov [c], Milana Vylegzhanina [c], Pavel Yakushev [b] & Yao Li [a]

[a] Center for Composite Materials, Harbin Institute of Technology, Harbin, P. R. China

[b] Ioffe Physical-Technical Institute, RAS, St.-Petersburg, Russia

[c] Institute of Macromolecular Compounds, RAS, St.-Petersburg, Russia

[d] Alan G. MacDiarmid Institute, Jilin University, Changchun, P. R. China

Accepted author version posted online: 01 Feb 2012.Published online: 09 Jul 2012.

To cite this article: Baode Zhang, Vladimir Bershtein, Tatiana Sukhanova, Wanchen Zang, Chunhai Chen, Larisa Egorova, Iosif Gofman, Galina Gubanova, Anatoly Volkov, Milana Vylegzhanina, Pavel Yakushev & Yao Li (2012) Aromatic Polyimide/MWCNT Hybrid Nanocomposites: Structure, Dynamics, and Properties, Journal of Macromolecular Science, Part B: Physics, 51:9, 1794-1814, DOI: 10.1080/00222348.2012.659640

To link to this article: http://dx.doi.org/10.1080/00222348.2012.659640

PLEASE SCROLL DOWN FOR ARTICLE

Taylor & Francis makes every effort to ensure the accuracy of all the information (the "Content") contained in the publications on our platform. However, Taylor & Francis, our agents, and our licensors make no representations or warranties whatsoever as to the accuracy, completeness, or suitability for any purpose of the Content. Any opinions and views expressed in this publication are the opinions and views of the authors, and are not the views of or endorsed by Taylor & Francis. The accuracy of the Content should not be relied upon and should be independently verified with primary sources of information. Taylor and Francis shall not be liable for any losses, actions, claims, proceedings, demands, costs, expenses, damages, and other liabilities whatsoever or

howsoever caused arising directly or indirectly in connection with, in relation to or arising out of the use of the Content.

This article may be used for research, teaching, and private study purposes. Any substantial or systematic reproduction, redistribution, reselling, loan, sub-licensing, systematic supply, or distribution in any form to anyone is expressly forbidden. Terms & Conditions of access and use can be found at http://www.tandfonline.com/page/terms-and-conditions

Downloaded by [Harbin Institute of Technology] at 18:47 28 December 2013

Journal of Macromolecular Science®, Part B: Physics, 51:1794–1814, 2012
Copyright © Taylor & Francis Group, LLC
ISSN: 0022-2348 print / 1525-609X online
DOI: 10.1080/00222348.2012.659640

Downloaded by [Harbin Institute of Technology] at 18:47 28 December 2013

Aromatic Polyimide/MWCNT Hybrid Nanocomposites: Structure, Dynamics, and Properties

BAODE ZHANG,[1] VLADIMIR BERSHTEIN,[2] TATIANA SUKHANOVA,[3] WANCHEN ZANG,[4] CHUNHAI CHEN,[4] LARISA EGOROVA,[2] IOSIF GOFMAN,[3] GALINA GUBANOVA,[3] ANATOLY VOLKOV,[3] MILANA VYLEGZHANINA,[3] PAVEL YAKUSHEV,[2] AND YAO LI[1]

[1]Center for Composite Materials, Harbin Institute of Technology, Harbin, P. R. China
[2]Ioffe Physical-Technical Institute, RAS, St.-Petersburg, Russia
[3]Institute of Macromolecular Compounds, RAS, St.-Petersburg, Russia
[4]Alan G. MacDiarmid Institute, Jilin University, Changchun, P. R. China

Two series of hybrid polyimide (PI)/multiwalled carbon nanotube (MWCNT) nanocomposites were prepared including COOH-functionalized or pristine nanotubes, and their structure, morphology and dynamics/mechanical properties at 20°C–500°C were studied using WAXD (Wide-angle X-ray diffraction), AFM (Atomic force microscopy), TEM (transmission electron microscopy), DSC (Differential scanning calorimetry), DMA (Dynamic mechanical analysis), CRS (creep rate spectroscopy) techniques, and stress–strain testing. The impact of nanofiller loadings of 0.125, 0.25, 0.5, or 1 wt% relative to PI was evaluated. Specific changes in the matrix morphology and different quality of nanotube dispersion in the nanocomposites with amorphous and semicrystalline matrices were determined. The best nanotube dispersion was observed in the composites with 0.5 wt% MWCNT-COOH. A peculiar high temperature dynamics, different for amorphous, and semicrystalline matrices, was revealed in these nanocomposites. The most dramatic changes in high temperature dynamics and a pronounced dynamic heterogeneity as well as substantially enhanced mechanical properties at room temperature were revealed in the case of a semicrystalline PI matrix. The results were treated in terms of the synergistic impact of nanotubes and matrix crystallites on dynamics in the intercrystalline regions of PI ("combined constrained dynamics effect") and the peculiar interfacial dynamics.

Keywords carbon nanotubes, hybrid nanocomposites, polyimide

Received 23 October 2011; accepted 8 December 2011.
Address correspondence to Vladimir Bershtein, Ioffe Physical-Technical Institute, RAS, St.-Petersburg194021, Russia. E-mail: vbersht@polmater.ioffe.ru; or to Yao Li, Center for Composite Materials, Harbin Institute of Technology, Harbin 150001, P. R. China. E-mail: liyao@hit.edu.cn

Downloaded by [Harbin Institute of Technology] at 18:47 28 December 2013

Introduction

Since their discovery by Iijima in 1991,[1] carbon nanotubes (CNTs) have attracted considerable attention because of their unique structure, excellent mechanical, thermal, magnetic and electric properties, in particular their extremely high strength to density ratio, and high chemical stability; this has made them the outstanding nanofillers for polymers. It has been shown in numerous studies that incorporation of CNTs into polymer matrices may substantially modify their properties and lead to nanocomposites with enhanced performance.[2,3] However, CNTs tend to form aggregates in organic media that may lead also to their inhomogeneous dispersion/distribution in a polymer matrix and negative impact on the properties of the resulting composites. In order to prevent CNT aggregation and to enhance interfacial interactions during fabricating the nanocomposites, special methods have been used including sonication for mixing of components and different ways for chemical functionalization of the CNT surface.[2–6]

Aromatic polyimides (PIs), as films and composite matrices, have attracted more and more attention owing to their excellent combination of high mechanical and dielectric properties, superior thermal/thermo-oxidative stability, as well as radiation, solvent and chemical resistance.[7,8] Therefore, PIs are used widely for the critical applications in a number of different areas, such as aerospace, electrical engineering, electronics, etc. However, the high performance applications require further enhancing PI properties in some cases, especially at ultrahigh temperatures. Potential improvements include increased strength, rigidity, and thermal and environmental stability. One of the main ways to achieve the enhanced PI properties is incorporating multiwalled carbon nanotubes (MWCNTs).[2,3]

Recently, PI/MWCNT nanocomposites with different PI matrices and compositions have been fabricated and investigated by a number of authors.[9–17] Rather different impacts of MWCNTs on PI properties have been observed depending on nanofiller content and functionalization, as well as the type of PIs and processing conditions. Through controlled variation of process parameters, various degrees of nanotube dispersion and distribution have been achieved. The dispersion/distribution states were correlated with the changes seen, in particular, in the glass transition temperature. Typically, the composites containing functionalized nanotubes exhibited better dispersion and mechanical properties than the corresponding composites containing pristine nanotubes. With the incorporation of functionalized MWCNTs, the mechanical properties of the resultant nanocomposite films were also improved in some cases due to enhancing the interfacial interactions between the modified MWCNTs and the PI matrix.

For instance, Shlea et al.[12] and Wu et al.[13] showed how the controlled morphology affected the nanocomposite properties, and the MWCNT dispersion and distribution could be changed by adjusting processing conditions. As a result, a substantial increase (e.g., from 324°C to 342°C) and some decrease or no change in glass transition temperature, T_g, were observed for the differently prepared PI/MWCNT nanocomposites; the latter negative effect was attributed to the presence of MWCNT agglomerates. It was found[14] that unmodified, acid-modified, and amine-modified MWCNTs had different influences on a PI matrix: the tensile strength of the PI/MWCNT composites increased with the acid-modified MWCNTs whereas the PI/unmodified MWCNT composites had better electrical conductivity. Chou et al.[15] showed that preliminary plasma-modification of MWCNTs, then grafting with maleic anhydride resulted in their good dispersion in the PI matrix and enhanced the thermal/mechanical properties and increased the conductivity at low nanotube content (below 0.5 wt%). It has also been shown that MWCNT additives could effectively

reduce friction and enhance antiwear capacity of PI.[16] The PI/MWCNT nanocomposites were sometimes electrically conductive at 3 wt% MWCNTs, which is favorable for some applications.[17]

Meantime, although a number of articles on PI/MWCNT nanocomposites have recently been published, the potential of reinforcement in these important nanocomposites has not been fully learned and realized, in our opinion, and an in-depth analysis of their structure and high-temperature dynamics is worth being performed.

The present work, devoted to the further experimental study of PI/MWCNT nanocomposites, is based on three experimental factors. First, two series of the nanocomposites, with amorphous and semicrystalline PI matrices, were studied in parallel. Secondly, one of the types of PI matrices (the amorphous one) included fluorine-containing groups. As known, PIs incorporating fluorinated groups in rigid nonplanar monomers exhibit an enhanced combination of mechanical and dielectric properties as well as transparency.[18,19] Additionally, the fluorinated groups in PI provide reduced moisture absorption and improved resistance to UV, charged particle radiation and atomic oxygen; these capabilities suit the extreme space conditions.[20,21] And third, a combined experimental approach, including the application of seven experimental techniques for studying simultaneously structure, morphology, dynamics, and mechanical properties of the nanocomposites at 20°C–500°C, was used in the present research.

Downloaded by [Harbin Institute of Technology] at 18:47 28 December 2013

Experimental

Materials

Pristine Materials. The AAPB (5-amino-2-(*p*-aminophenyl) benzoxazole (purity 99.71%, melting point 230.0°C–230.6°C) was prepared at Harbin Institute of Technology (Harbin, China). 6FDA (4,4′- hexafluoroisopropyl diphthalic anhydride, melting point 248°C) was obtained from Fluorochem Ltd (Derbyshire, UK). ODPA (4, 4′-oxydi-phthalic anhydride, purity 99.7%, melting point 227.3°C) was received from Shanghai Research Institute of Synthetic Resins (China). N, N-dimethylacetamide (DMAc) was distilled before use.

The MWCNTs had been synthesized by catalytic chemical vapor deposition (CVD technology) of acetylene over Fe loaded mesoporous silica. Both pristine MWCNTs with outer diameter of 30–50 nm, inner diameter 5–12 nm, and length of 10–20 μm, and COOH-functionalized nanotubes (MWCNT-COOH) were obtained from Chengdu Organic Chemicals Co. Ltd., Chinese Academy of Science. The raw product contained the aerogel support, catalyst particles, and a small amount of amorphous carbon as impurities. The as-grown MWCNTs were purified using a three-step procedure involving acid etching, oxidation, and graphitization under inert gas for 20 h at 2800°C. These MWCNTs were characterized by thermogravimetric analysis (TGA), scanning electron microscopy (SEM), transmission electron microscopy (TEM), and energy dispersive spectrometry (EDS). It was shown that most of the mesoporous silica and metal particles were removed from the as-grown MWCNTs by these treatments. Neat MWCNTs (purity 99.9%) and then MWCNT-COOH, obtained by their treatment with $KMnO_4$, were used.

Preparation of the PIs and PI/MWCNT Nanocomposites. To obtain PIs PI(AAPB-6FDA) (PI-I) or PI(AAPB-ODPA) (PI-II) with the formulas respectively, and the nanocomposites based thereon, AAPB was dissolved in DMAc at room temperature and then sonicated after adding MWCNTs. The dilute MWCNT-COOH or MWCNT suspension was obtained by sonication for 3 h at 47 kHz. The suspension was immediately transferred to a nitrogen

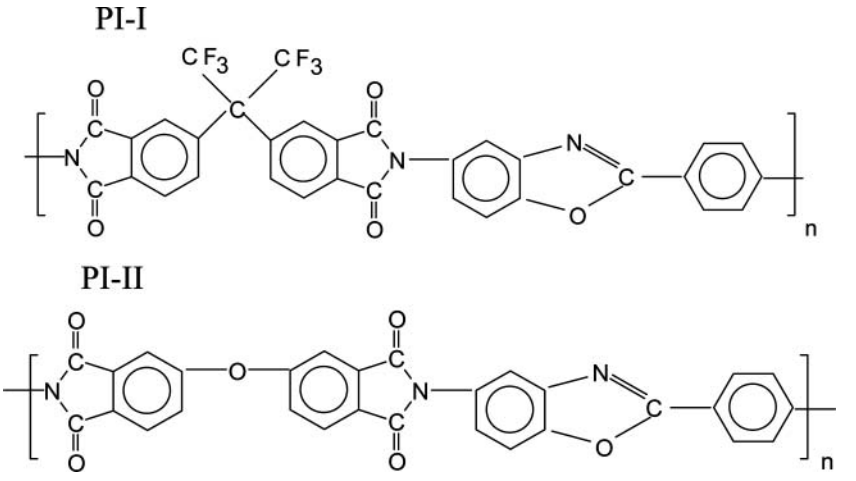

purged three-neck round bottom flask equipped with a mechanical stirrer and drying tube outlet filled with calcium sulfate. After stirring the MWCNTs dispersion, 6FDA, or ODPA was added. The reaction mixture was sonicated in a bath sonicator while simultaneously being stirred 6 h at 300 rpm at room temperature until the solution viscosity increased and stabilized. Sonication was then stopped with a MWCNT-poly(amic acid) (PAA) solution having been formed. The DMAc solutions of PAA (with or without MWCNTs) were cast onto clean glass plates and dried in a dry air-flowing chamber for 10 h at 90°C. Then the films, with a thickness of 40–60 μm, were step-wise cured in vacuum at temperatures up to 350°C to obtain fully imidized, solvent free PI/MWCNT films.

In this work, the impact of loadings, $c = 0.125$, 0.25, 0.5, or 1 wt% COOH-functionalized MWCNTs relative to PI were evaluated. For comparison, the nanocomposites with 0.5 and 1 wt% nonfunctionalized MWCNTs were also studied.

Characterization

Wide-Angle X-Ray Diffraction (WAXD). Wide-angle X-ray analysis was made using the diffractometer Seifert XRD 3003 TT (GE, Germany), which was supplied with a primary monochromator; CuK_α radiation with wavelength $\lambda = 1.54$ Å was used. All diffractograms were obtained in the range of scattering angles $2\theta = 2°$–$40°$ with steps of 0.05°, and time of scanning equal to 5 s for each point in the scattering angles range.

Atomic Force Microscopy (AFM). The morphology of the nanocomposite films, including dispersion quality of MWCNTs in the matrix, was examined by AFM using a Nanotop NT-206 instrument (Microtestmashiny, Gomel, Belarus) in a tapping mode. The topographic images, surface profiles and amplitude images were obtained.

Transmission Electron Microscopy (TEM). The TEM images were obtained using a Hitachi H-7650 field emission transmission electron microscope (Japan) at an acceleration voltage of 100 kV. The films of nanocomposites were embedded into epoxy resin Epon-812 (Houston, TX, USA), then the samples were cut into slices of ~80 nm thickness using a RMC PowerTome XL Ultramicrotome with a diamond knife (Boeckeler Instruments, Tucson, AZ, USA) and were collected on round 400 mesh copper grids.

Downloaded by [Harbin Institute of Technology] at 18:47 28 December 2013

Dynamic Mechanical Analysis (DMA). Dynamic viscoelasticity of the nanocomposites was analyzed in tension mode at 1 Hz using a Dynamic Mechanical Spectrometer DMS 6100 Seiko Instruments (Japan) at temperatures from 20°C to 510°C. A sample was heated at the rate of 3°C min^{-1}. Tensile loss modulus E'', tensile storage modulus (dynamic modulus) E', and mechanical loss factor $\tan\delta = E''/E'$ as functions of temperature were measured. It should be noted that these values were measured at very low stresses ($\leq$1 MPa).

Differential Scanning Calorimetry (DSC). A Perkin–Elmer DSC-2 apparatus (Waltham, MA, USA) was used for glass transition characterization of the materials studied. Glass transition temperatures, including T_g at the half-height of a heat capacity step ΔC_p, the temperatures of transition onset, T_g', and completion, T_g'', as well as the values of ΔC_p were determined. The DSC measurements were performed in nitrogen atmosphere over the temperature range from 20°C to 500°C. Sample mass was 28 mg, and amorphous quartz was used as a reference sample. To exclude the impact of absorbed water and sample prehistory, scans I, II, and III were performed during heating with the rate $V = 20$°C min^{-1}, first from 20°C to 400°C (scan I) and then from 20°C to 500°C (scans II and III); cooling was performed at $V = 320$°C min^{-1}.

Laser-Interferometric Creep Rate Spectroscopy (CRS). The CRS, as a high-resolution method of relaxation spectrometry and thermal analysis, allowed us to characterize in a discrete way the dynamics, dynamic heterogeneity and creep resistance of the materials over a broad temperature region; the CRS setups and experimental technique have been described in detail elsewhere.[22] This technique consists in precisely measuring creep rates at a constant low stress, much less than the yield stress, as a function of temperature (creep rate spectrum). For this purpose, a laser interferometer based on the Doppler effect is used. The time evolution of deformation is registered as a sequence of low-frequency beats in an interferogram whose beat frequency, ν, yields a creep rate

$$\dot{\varepsilon} = \frac{\lambda \nu}{2I_0} \tag{1}$$

Here, $\lambda = 630$ nm is the laser wavelength, and I_0 is the initial length of the working part of the sample. Film samples with 1×5 mm^2 cross-section and 5-cm length were used. The creep rate spectra were measured over the temperature range from 20°C to 460°C at a tensile stress of 3 or 5 MPa (see below). A stress was chosen in the preliminary experiments as capable of inducing sufficient creep rates to be measured, while maintaining also a high spectral resolution, without smoothing out or distortion of a spectral contour and preventing premature rupture of a sample. While heating with the rate $V = 1$°C min^{-1}, every 5°C the sample was loaded, and an interferogram was recorded 10 s after loading; then the sample was unloaded, and the experiment repeated 5°C higher. The instrumental error in measuring creep rates did not exceed 1% but scattering in the peak height and temperature location may attain 20% and 3°C–5°C, respectively, during measuring identical samples.[22] The correlative frequency of the CRS experiments was $\nu_{corr} = 10^{-3}$ to 10^{-2} Hz.

Stress-Strain Testing. The mechanical tests of the films under study at room temperature were carried out in the uniaxial extension mode using a universal mechanical test system. The strip-like samples, with the dimensions of the part under test of 2×30 mm^2, were tested with an extension speed of 10 mm/min according to ASTM D638. The Young's modulus, E, the yield stress, σ_y, the break stress, σ_b, and the ultimate deformation, ε_b, were determined.

Downloaded by [Harbin Institute of Technology] at 18:47 28 December 2013

Downloaded by [Harbin Institute of Technology] at 18:47 28 December 2013

Results and Discussion

Matrix Structure/Morphology and MWCNT Dispersion

The WAXD patterns obtained for PI-I and the nanocomposites based thereon are shown in Fig. 1. One can see that this polymer was characterized by one broad peak, centered at $2\theta = 14^\circ$, indicating its amorphous structure. Introducing 0.25–1.0 wt% nanotubes did not change this peak that suggests an unchangeable matrix structure in these nanocomposites. However, a very weak and broad peak was also present at $2\theta = 25^\circ$–30° for the PI-I-based nanocomposites. This peak may correspond to the turbostratic carbon structure of MWCNTs; the intershell spacing in MWCNTs is equal to 3.40 Å being quite close to the interlayer spacing in turbostratic graphite.[23] However, such manifestation of very low MWCNT content is a surprising fact, and it is impossible to exclude also a contribution to the peak at $2\theta = 25^\circ$–30° from a second "amorphous peak" (as observed earlier in amorphous polymers[24]), related to a spacing along the chains.

In contrast, the WAXD patterns presented in Fig. 2 show that PI-II had a semicrystalline structure since two intense peaks at $2\theta = 13.9^\circ$ and 17.8°, corresponding to the interlayer spacings of $d = 6.35$ and 4.98 Å, respectively, and also the less intense peak at 26.2° corresponding to $d = 3.40$ Å, were observed in both neat PI-II and the nanocomposites based thereon. The latter peak appears to be larger in curves 1 and 3–5 whereas it is lower and identical for neat PI-II (curve 6) and the nanocomposite with 0.5 wt% MWCNT-COOH (curve 2). Thus, introducing 0.25–1.0 wt% nanotubes into PI-II changed differently the ratio of the peak intensities, mostly at $2\theta = 13.9^\circ$ and 17.8°.

When analyzing these changes, it should be mentioned again that the peak at $\sim 26^\circ$ may be characteristic of both matrix structure and MWCNTs. Therefore, increasing intensity of this peak in the nanocomposites may be associated with both some aggregation of MWCNTs and the structural changes in the matrix. The redistribution of peak intensities at 13.9° and 17.8° indicates the structural changes.

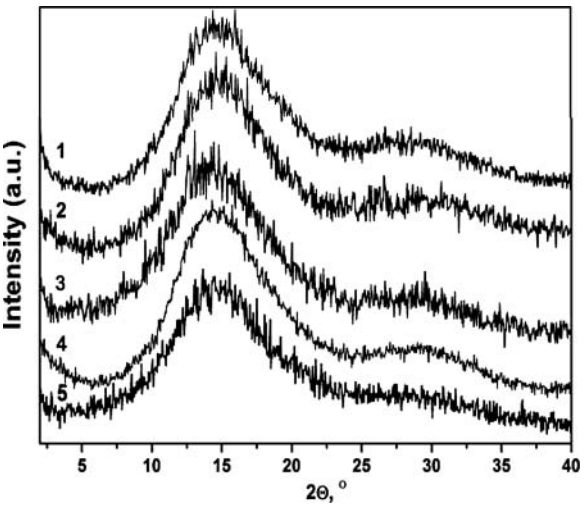

Figure 1. The WAXD patterns for PI-I-based nanocomposites with (1) 1 wt% MWCNT; (2) 1 wt% MWCNT-COOH; (3) 0.5 wt% MWCNT-COOH; (4) 0.25 wt% MWCNT-COOH and for neat PI-I (5).

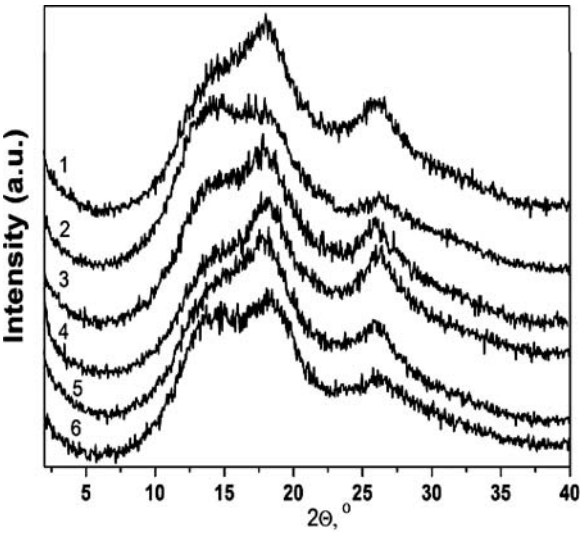

Figure 2. The WAXD patterns for PI-II-based nanocomposites with (1) 1 wt% MWCNT-COOH; (2) 0.5 wt% MWCNT-COOH; (3) 1 wt% MWCNT; (4) 0.5 wt% MWCNT; (5) 0.25 wt% MWCNT-COOH, and for neat PI-II (6).

Thus, Fig. 2 shows that the smallest changes compared with neat PI-II (curve 6) were observed in the WAXD pattern of the nanocomposite with 0.5% MWCNT-COOH (curve 2); in particular, the peak intensity at $\sim 26^\circ$ did not change suggesting rather slight structural changes in the PI-II matrix and presumably the best dispersion of MWCNT-COOH in this composite. Contrarily, introducing 0.5% nonfunctionalized MWCNTs (curve 4), or 1% functionalized or pristine MWCNTs (curves 3 and 5) resulted in considerable changing of the WAXD pattern, in particular increasing the peak intensity at $\sim 26^\circ$.

The AFM and TEM data obtained are in a satisfactory accordance with these observations. The representative AFM images in "topographic" and "amplitude" modes of surface morphology as well as surface profiles (along the marked dotted lines in the topographic images) of the PI/MWCNT nanocomposites and neat PI matrices are presented in Figs. 3 and 4.

Figures 3a, d, and g present the AFM topographic images of the free surfaces of pure PI-I film (a) and nanocomposite samples containing 0.5 wt% unmodified (d) or modified MWCNTs (g) in the amorphous PI-I matrix. It is obvious that there are differences in the morphology of samples under study and in the quality of the MWCNT dispersion. Comparison of these AFM images shows that the most plane morphology with a small profile roughness (highest peaks up to 2–3 nm, Fig. 3b), likely determined by clusters of PI macromolecules, was exhibited by the pure PI-I film. Despite the comparatively smooth morphology, the free surface of the PI-I film had a lot of 10–50 nm sized pores (Fig. 3a) that clearly correlates with the imidization water and the residual solvent elimination during the thermal processing of the film.

In the case of unmodified nanotubes (Figs. 3d—f), the dispersion of MWCNTs in the PI-I matrix was poor (the bright areas in the image of Fig. 3d can be attributed to the MWCNT aggregates), and aggregates up to 50 nm in height (Fig. 3e) and 200 to 500 nm in diameter appear. Additionally, it may be assumed from the AFM images (d, f), and also TEM images presented later, that the unmodified MWCNTs have a tendency to roll up, be highly crimped and interwoven, creating agglomerates within the PI-I matrix. As a result, the topography formed in the PI-I/MWCNT (0.5 wt%) composite (Fig. 3d) had

Downloaded by [Harbin Institute of Technology] at 18:47 28 December 2013

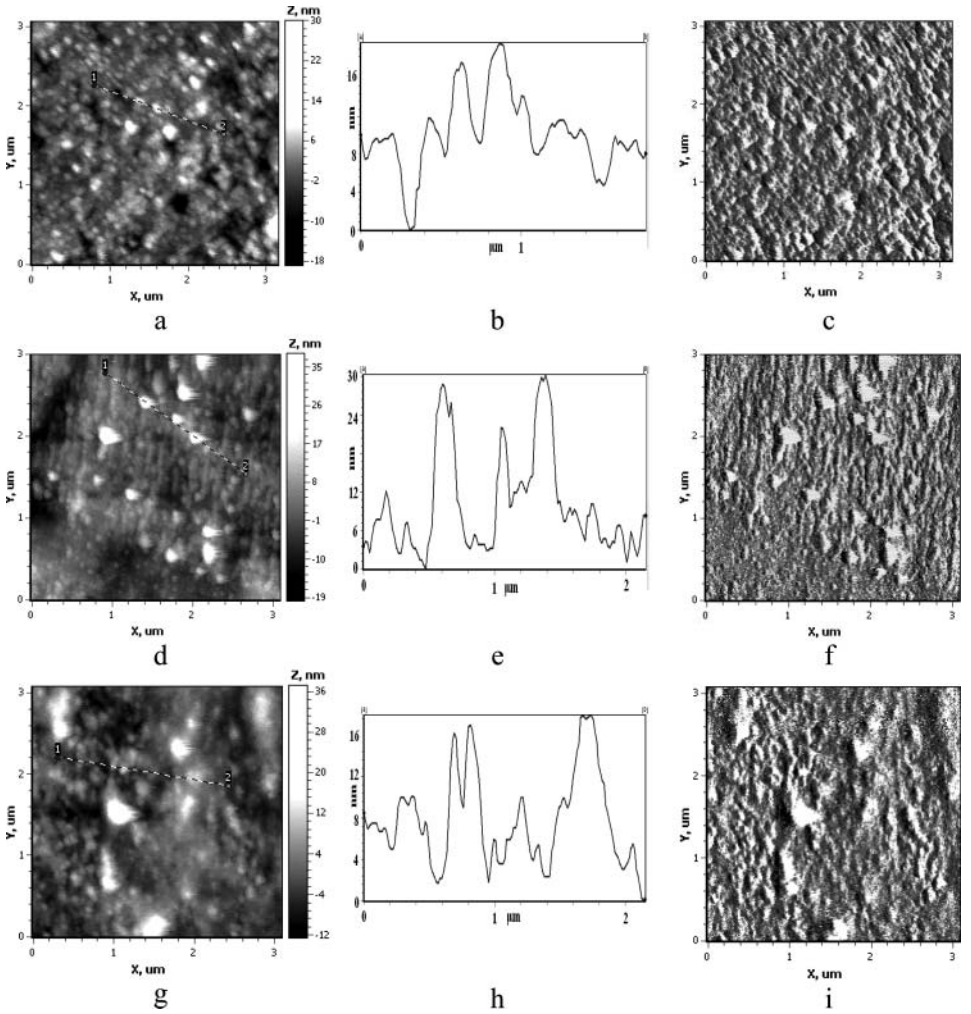

Figure 3. The AFM images obtained in tapping mode for (a–c) pure PI-II, (d–f) PI-II/MWCNT (0.5 wt%), and (g-i) PI-II/MWCNT-COOH (0.5 wt%) composites. a, d, g—topographic images; b, e, h—profiles; c, f, i—amplitude images.

a pronounced, nonsmooth relief in which the MWCNT agglomerates embedded in the PI matrix protrude over the PI-I film surface.

Unlike the case of the unmodified MWCNTs, a greatly improved dispersion of MWCNT-COOH (0.5 wt%) was observed within the PI-I matrix (see, e.g., a relief in Fig. 3h). This is probably due to strong interfacial interactions and chemical compatibility between the PI matrix and the modified MWCNTs during nanocomposites preparation (see below).

AFM amplitude images (Figs. 3c, f, and i), which are the error signal in the feedback loop controlling tip height and accentuate changes in the surface relief height,[25] and their profiles (Figs. 3b, e, and h) also show that introducing the unmodified (d–f) and modified (g–i) MWCNTs into the PI-I matrix significantly changed the film morphology, its roughness and voids content. It can be seen that the modified nanotubes were practically individually separated and uniformly dispersed in the PI-I/MWCNT-COOH (0.5 wt%)

Downloaded by [Harbin Institute of Technology] at 18:47 28 December 2013

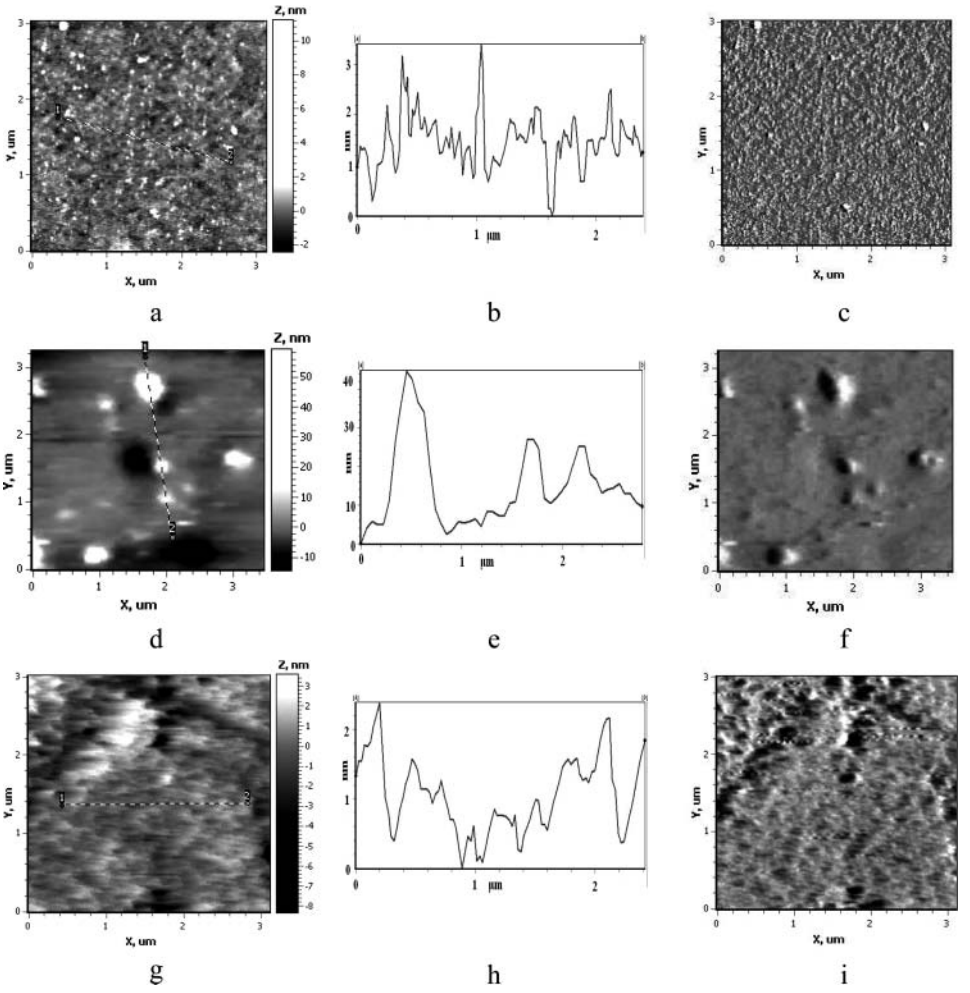

Figure 4. The AFM images obtained in tapping mode for (a–c) pure PI-I, (d–f) PI-I/MWCNT (0.5wt%) and (g–i) PI-I/MWCNT-COOH (0.5 wt%) composites. a, d, g—topographic images; b, e, h—profiles; c, f, i—amplitude images.

composite film (Fig. 3g) with all the MWCNT-COOH tips coated by polymer revealed on the free film surface. This film displayed a comparatively smooth relief (highest peaks up to 4 nm, Fig. 3g and h) and only a few voids. No obvious nanotube agglomeration in this composite, unlike the aggregation of untreated MWCNTs, can be observed.

The surface morphology of the nanocomposite films based on semicrystalline PI-II exhibited another behavior. The free surface of the pure PI-II film had a "knobby" texture (Figs. 4a and c) resembling a sub-structure, which has been visualized previously by AFM method in other semicrystalline polymers,[26,27] with knobs 30–100 nm in diameter and profile roughness determined by the PI crystallites (highest peaks up to 15–20 nm, Fig. 4b). On the PI-II film surface, a much more pronounced porosity, in comparison with the amorphous PI-I film, was observed, with nano- and mesopores from 20 to 300 nm in diameter (Figs. 4a–c).

Downloaded by [Harbin Institute of Technology] at 18:47 28 December 2013

The free surface of the sample containing unmodified 0.5 wt% MWCNTs (Fig. 4d) again displayed mainly aggregates of 150–200 nm in size composed of several nanotubes and some separated MWCNTs that were distributed along specific paths (in vertical direction in Figs. 4d and f), instead of larger isolated MWCNT agglomerates within the amorphous PI-I matrix (Figs. 3d and f).

In the case of modified MWCNTs embedded in the PI-II matrix, besides nanotubes which were individually separated and uniformly dispersed in the PI-II/MWCNT-COOH (0.5wt%) composite film, a few aggregates were revealed on the free film surface (Figs. 4g and i). Therefore, one can conclude that crystallizability of the PI-II matrix prevents, to some extent, the uniform dispersion of MWCNTs even after their functionalization. The MWCNT-COOH were located, undoubtedly, within the disordered layers between the PI-II crystallites.

The nanotube dispersion in the PI matrices was also examined by TEM. These results confirmed that unmodified MWCNTs in the PI-I matrix (mass fraction was 0.5 wt%) tangled with each other in their original state and formed aggregates of different sizes and shapes (Fig. 5a) due to the van der Waals attraction between the MWCNTs. In contrast with the untreated MWCNTs (0.5 wt%) reinforced PI-I composite, modified nanotubes in the PI-I/MWCNT-COOH (0.5 wt%) composite were distributed uniformly and separately from one another (Fig. 5b), owing to the strong interfacial interactions between the surface

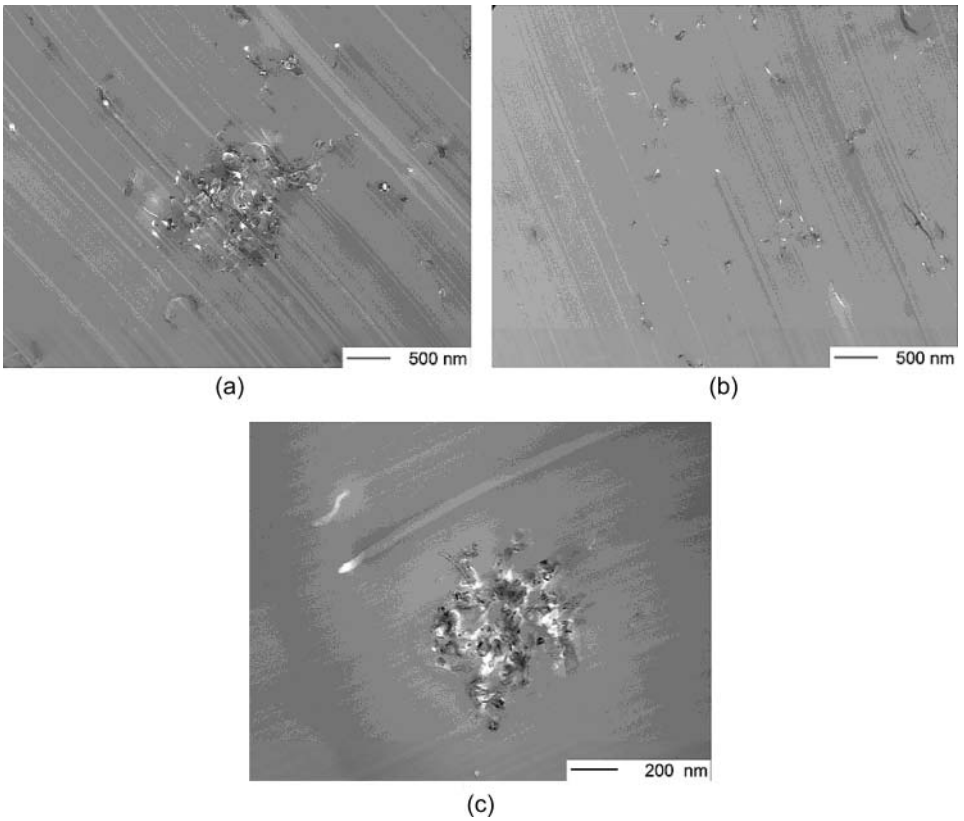

Figure 5. Typical TEM images of PI-I-based nanocomposites with (a) 0.5 wt% MWCNT; (b) 0.5 wt% MWCNT-COOH, and (c) 1 wt% MWCNT-COOH.

Downloaded by [Harbin Institute of Technology] at 18:47 28 December 2013

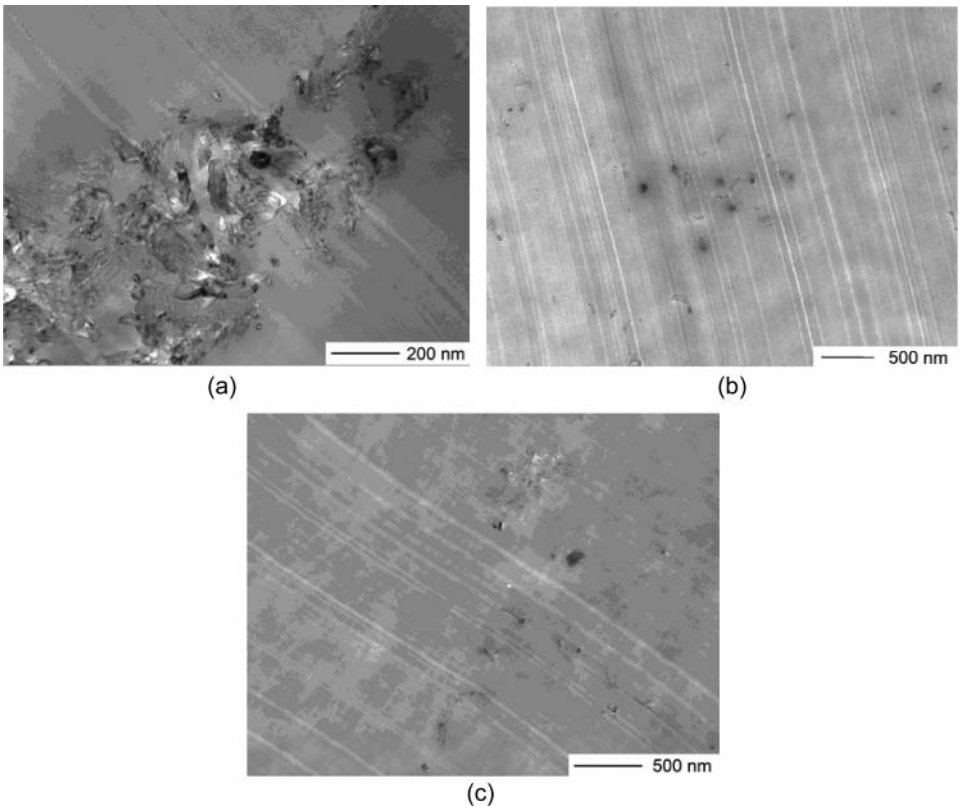

Figure 6. Typical TEM images of PI-II-based nanocomposites with (a) 0.5 wt% MWCNT; (b) 0.5 wt% MWCNT-COOH, and (c) 1 wt% MWCNT-COOH.

carboxylic groups of the nanotubes and the PI-I matrix. However, with increasing MWCNT-COOH concentration, up to 1 wt%, they began to agglomerate to some extent (Fig. 5c).

The TEM images show that, in the case of the semicrystalline PI-II matrix, the dispersion of 0.5 wt% unmodified MWCNTs was poor; large "friable" aggregates were observed (Fig. 6a). On the other hand, the modified MWCNT-COOH were better dispersed within the PI-II matrix at both 0.5 and 1 wt% nanotubes although the best dispersion was again observed at 0.5% (Fig. 6b).

Dynamics and Properties of the Amorphous PI(AAPB-6FDA)-Based Nanocomposites

Figure 7, a shows the DMA spectra obtained for PI-I and a few nanocomposites based thereon. The relatively narrow glass transition peak within the ∼330°C–370°C range, peculiar to this amorphous PI-I, retains practically an invariable temperature position with the maximum at 350 ± 5°C and only slightly varying maximal mechanical loss level in the nanocomposites. Introducing MWCNTs resulted in a large rise of dynamic heterogeneity within or close to the glass transition: the relaxation spectrum contour substantially changed at both higher and lower temperatures beyond the 330°–370° range. Thus, a broad high temperature "wing" over the 380°C–500°C range and a maximum at ∼480°C developed in the nanocomposites′ spectra. This may be assigned to manifesting the different degrees of constraining segmental dynamics[22,28] in PI-I nanovolumes located at or close to (at

Downloaded by [Harbin Institute of Technology] at 18:47 28 December 2013

Downloaded by [Harbin Institute of Technology] at 18:47 28 December 2013

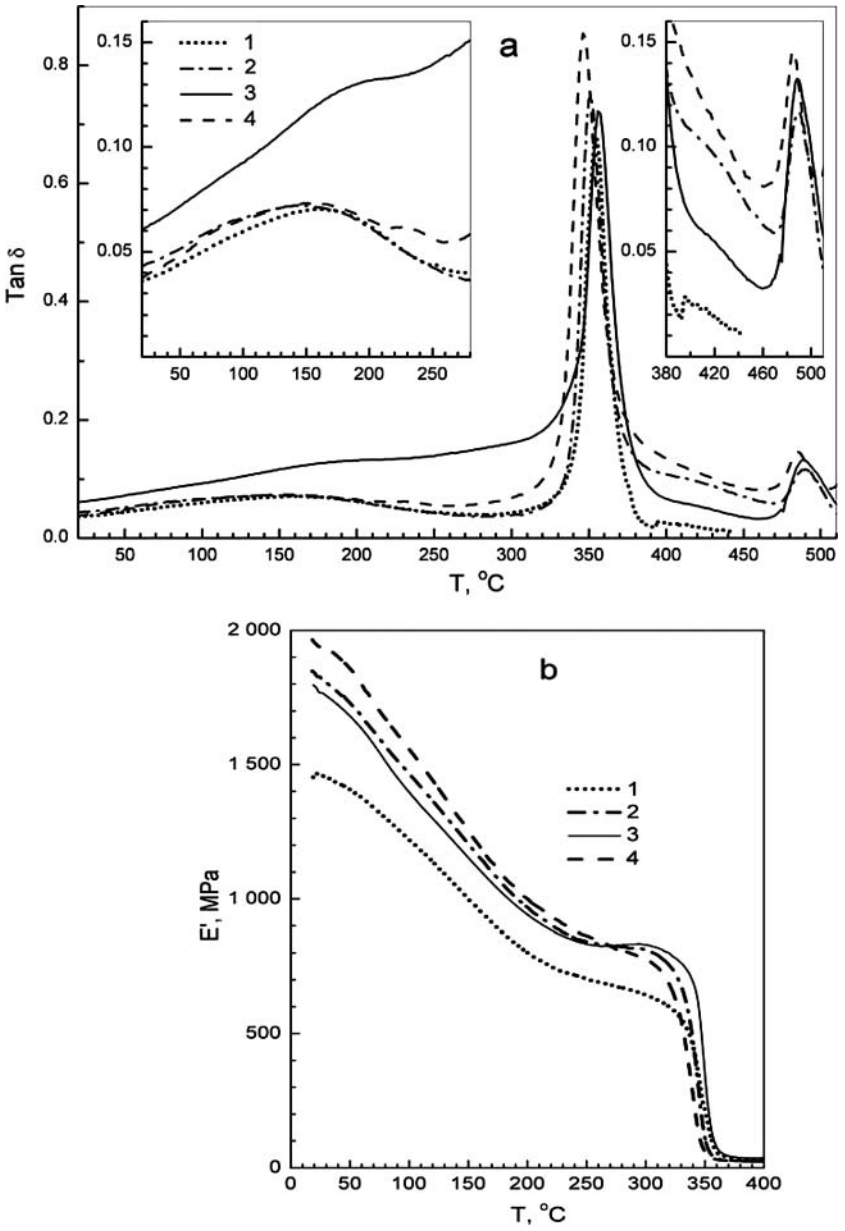

Figure 7. The DMA (1 Hz): (a) mechanical loss spectra and (b) dynamic modulus E' vs. temperature dependencies obtained for (1) neat PI-I and PI-I-based nanocomposites with (2) 0.25 wt% MWCNT-COOH, (3) 0.5 wt% MWCNT-COOH, and (4) 1 wt% MWCNT-COOH.

different distances from) the phase interfaces in the nanocomposites. Such an effect is due to the enhanced interfacial interactions in the nanocomposites that are associated, obviously, not only with development of the hydrogen bonds between the COOH-groups of the modified MWCNT surface and PI-I macromolecules: because of the PIs being synthesized in the presence of nanotubes; chemical reaction between the amine groups of AAPB and the carboxyl "cover" of the MWCNTs may also occur to some extent. We suggest that covalent

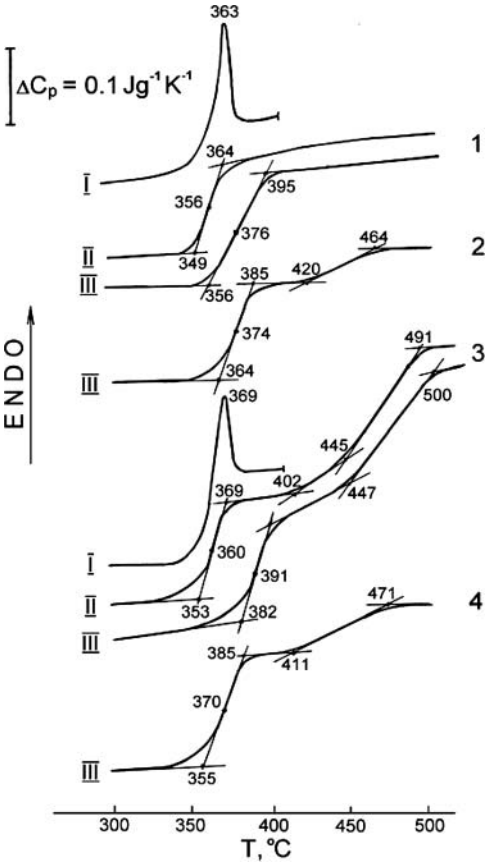

Figure 8. The DSC curves obtained for (1) neat PI-I and PI-I-based nanocomposites with (2) 0.25 wt%, (3) 0.5 wt%, and (4) 1 wt% MWCNT-COOH. Scan I was performed at temperatures from 20°C to 400°C, and heating scans II and III–up to 500°C. Heating and cooling rates were 20°C and 320°C min^{-1}, respectively.

bonding at the interfaces may be responsible for the largest constrained dynamics effect resulting in presence of the relaxation peak at 480°C; this peak characterizes, obviously, "unfreezing" suppressed interfacial dynamics in these nanocomposites.

On the other hand, increasing mechanical losses took place, also, at temperatures below the main glass transition in the nanocomposites, especially for the composite with 0.5 wt% modified MWCNTs (Fig. 7a). Unlike the broad β-relaxation peaks with the maxima at 140°C–150°C observed for the other composites, enhanced mechanical losses over the range from 20 to 330°C (β- and "intermediate" relaxations) and the displacement of the β-maximum to 180°C was seen for this composite. These effects may, apparently, be caused, besides constraining PI dynamics by the MWCNTs (the latter shift), by two other reasons: loosening of the molecular packing and less perfect imidization, locally, due to some consumption of amine groups of AAPB by chemical interaction with COOH-groups of MWCNT surface. Figure 7b, showing dynamic modulus data, will be discussed below.

DSC curves presented in Fig. 8 confirm, additionally, the complicated, two-mode dynamics within the glass transition region in the PI-I–based nanocomposites: besides the main transition at ~350–370°C, a large heat capacity step, ΔC_p, in the temperature

Downloaded by [Harbin Institute of Technology] at 18:47 28 December 2013

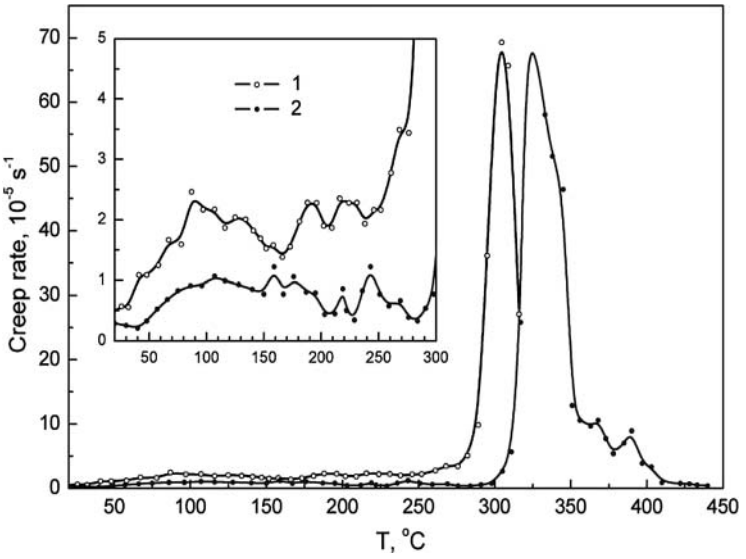

Figure 9. Creep rate spectra obtained at tensile stress 3 MPa for (1) neat PI-I and (2) PI-I/ MWCNT-COOH (0.5 wt.%).

range of ∼400–500°C was also registered. The latter effect of manifesting the peculiar interfacial dynamics was the strongest for the PI-I/MWCNT-COOH (0.5%) composite having the best nanotube dispersion. In addition, scans III, performed after heating the samples up to 500°C, show also the possibility of the additional increase of T_g in the main transition, at the limit from 360 to 391°C for the composite with 0.5% MWCNT-COOH. It is interestingly to compare the data presented in Figs. 8 and 7a: an unexpectedly large ratio of two ΔC_p steps, at ∼400–500 and 350°C–370°C, was observed for the composite with 0.5% MWCNT-COOH. This directly indicates the increased heat required for unfreezing interfacial dynamics at temperatures over 400°C compared with the "usual" heat needed for unfreezing dynamics in the main transition.

Figure 9 shows the discrete creep rate spectra of neat PI-I and the PI-I/MWCNT-COOH(0.5%) nanocomposite. The main glass transition peaks are located at lower temperatures than DMA peaks and DSC heat capacity steps. In addition, one can see again the constrained dynamics effect caused by introducing MWCNTs. It manifests itself as the displacement of the basic T_g peak by ∼25°C to higher temperatures, the appearance of the higher-temperature "wing" at 350°C–400°C in the spectrum, and decreasing creep rates in the temperature regions of the β -relaxation (∼50°C–150°C) and "intermediate relaxations" (∼150–250°C) in the nanocomposite spectrum.

Finally, Fig. 7b shows the tensile dynamic modulus E' vs. temperature dependencies obtained by DMA (1 Hz) for neat PI-I and a few nanocomposites. One can see that introducing functionalized MWCNTs into PI-I resulted in an E' increase by ∼20%–30% over the broad temperature range of the nanocomposite glassy state, from 20°C to 300°C; maximal E' values were observed for 1 wt% MWCNT-COOH.

Dynamics and Properties of the Semicrystalline PI(AAPB-ODPA)-Based Nanocomposites

The nanocomposites with semicrystalline PI-II matrix exhibited the different dynamic behavior than the amorphous PI-I-based composites. Figure 10a shows the DMA spectra

Downloaded by [Harbin Institute of Technology] at 18:47 28 December 2013

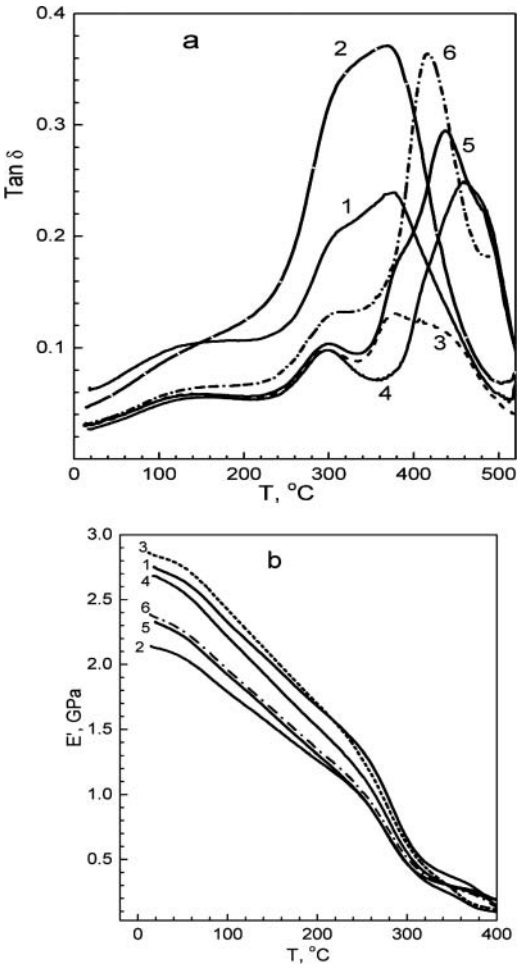

Figure 10. The DMA (1 Hz): (a) mechanical loss spectra and (b) dynamic modulus E' vs. temperature dependencies obtained for (1) neat PI-II and PI-II-based nanocomposites with (2) 0.125 wt% MWCNT-COOH, (3) 0.25 wt% MWCNT-COOH, (4) 0.5 wt% MWCNT-COOH, (5) 1 wt% MWCNT-COOH, and (6) 1 wt.% MWCNT.

of neat PI-II and the nanocomposites based thereon. The spectrum of the neat matrix was characterized by, besides a relatively slight and broad β-relaxation peak with a maximum at 100°C–150°C, a broad, complicated glass transition peak covering the temperature region between 250°C and 480°C (curve 1). This tan δ peak is, in fact, the sum of two strongly overlapping peaks with their maxima at 290–300 and 370°C. If the former constituent peak may be related to the amorphous phase, the latter one characterizes, evidently, the hindered, by crystallites, cooperative segmental motion in the disordered PI-II regions, i.e., it may be treated as the manifestation of the constrained dynamics [22,28] or, in another terms, of the "rigid amorphous fraction (RAF)"[29] coexisting along with the rigid crystalline and usual, "soft" amorphous phases.

Figure 10a shows that adding of nanotubes resulted, depending on their content c, in absolutely different, dramatic changes of the glass transition dynamics in the PI-II matrix. Thus, at $c = 0.125\%$ MWCNT-COOH a twofold increase of both overlapping peaks was

Downloaded by [Harbin Institute of Technology] at 18:47 28 December 2013

observed (curve 2) that we attribute to enhancement of the mobility due to some loosening of molecular packing. In contrast, the effect of suppression of PI-II mobility mainly prevails at larger nanotube contents. At $c = 0.25\%$ MWCNT-COOH, the temperature location of both peaks remained unchanged but their intensities and the loss level over the range from 20°C to 430°C strongly decreased (curve 3); in addition, some tendency for the appearance of an additional peak at 430°C may be seen. With increasing c up to 0.5% or 1% MWCNT-COOH the lower-temperature constituent glass transition peak did not change whereas the higher-temperature relaxation peak increased in height and shifted strongly to higher temperatures, viz., from 370° to 460° (curve 4) or 440°C (curve 5), respectively. A shoulder at 370°C was observed in curve 5 as the remainder of initial peak undisturbed by nanotubes. At the same time, at $c = 1\%$ nonfunctionalized MWCNTs, the high-temperature mobility (mechanical loss level) of the nanocomposite also increased but the latter peak had a maximum at 420°C (curve 6). These results reflect the impact of different interfacial interactions (functionalized or nonfunctionalized MWCNTs) on the glass transition dynamics and the best dispersion for 0.5% MWCNT-COOH.

Thus, location of the lower-temperature glass transition peak, corresponding to segmental dynamics in the amorphous nanoregions undisturbed by crystallites, remains practically unchangeable (290°C–300°C) for the composites with 0.5% or 1% MWCNT-COOH. The effect of very strong and different displacement of the second constituent peak to higher temperatures can be tentatively treated, in our opinion, in terms of the synergistic impact of MWCNTs and PI crystallites, as "rigid constraints" covalently connected with the PI disordered nanoregions, on the glass transition dynamics within the RAF of the matrix. This "combined constrained dynamics effect" takes place, obviously, first of all at PI-II-nanotube interfaces. Due to the better nanotube dispersion, the PI/MWCNT-COOH (0.5%) hybrid may be considered, to a certain extent, as the "interface-controlled material". Figure 10b, showing dynamic modulus data, will be discussed below.

Qualitatively similar manifestation of dynamics in the nanocomposites under consideration was also recorded by the two glass transitions in the DSC curves (Fig. 11). Thus, the distinct effect of suppressing the dynamics by nanotubes was registered for the PI-II-MWCNT-COOH (0.5%) nanocomposite: the lower-temperature heat capacity step decreased and its width changed, compared with neat PU-II, from 63°C (curve 1) to 37°C (curve 2), whereas the higher-temperature heat capacity step started at 438°C but at 407°C for neat PI-II. Increasing nanotube content up to 1 wt% results in the opposite effects of decreasing temperatures and broadening transitions, attributed to larger nanotube aggregation. One can also see some difference in the thermal behavior of the nanocomposites with modified and nonfunctionalized MWCNTs (curves 3 and 4). It should be noted that DSC did not allow registering the completion of the higher-temperature transition for PI-II and the nanocomposites based thereon, due to some overlapping of the higher-temperature heat capacity step with the side endothermic effect caused by the onset of matrix destruction. The latter process started from the interfacial layers since a gradual decrease of the intensity (slope) of the higher-temperature step was observed in the repeated scans up to 500°C (not shown here).

Figure 12 compares two creep rate spectra obtained for neat PI-II and the nanocomposite with 0.5 wt% MWCNT-COOH. The discrete spectrum of the neat matrix included at least seven overlapping constituent peaks with different intensities, indicating the pronounced dynamic heterogeneity within the glass transition range (peaks at ~340°C, 360°C, 390°C, and 410°C), and covering the regions of the "intermediate relaxations" (peak at 200°C–250°C), and the β-relaxation (peaks at 90°C and 150°C). Such strong dynamic heterogeneity within the glass transition is peculiar to semicrystalline PIs; this has earlier

Downloaded by [Harbin Institute of Technology] at 18:47 28 December 2013

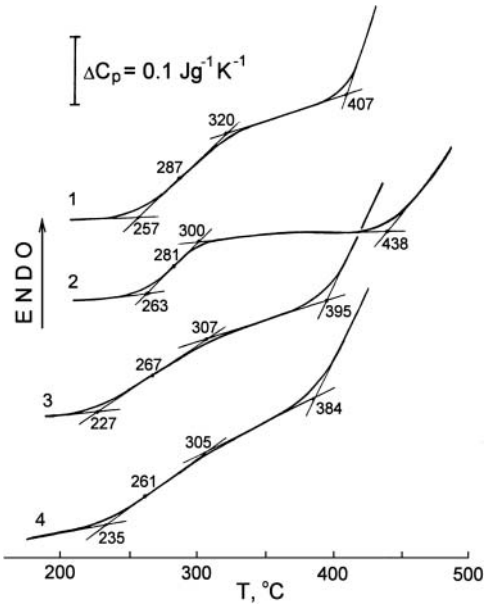

Figure 11. The DSC curves obtained for (1) neat PI-II and PI-II-based nanocomposites with (2) 0.5 wt% MWCNT-COOH, (3) 1 wt% MWCNT-COOH, and (4) 1 wt% MWCNT. Scan II at the heating rate 20°C min^{-1} after heating up to 500°C and subsequent cooling with the rate 320°C min^{-1}.

been demonstrated by CRS for other PIs with the complicated morphologies including disordered, mesomorphous, and crystalline nanophases.[30] This multimodal segmental dynamics suggests the presence of a few discrete levels of the molecular packing density and constrained dynamics effects in the PI micro- or nanodomains. Figure 12 confirms that introducing 0.5% MWCNT-COOH into PI-II results basically in additional constrained

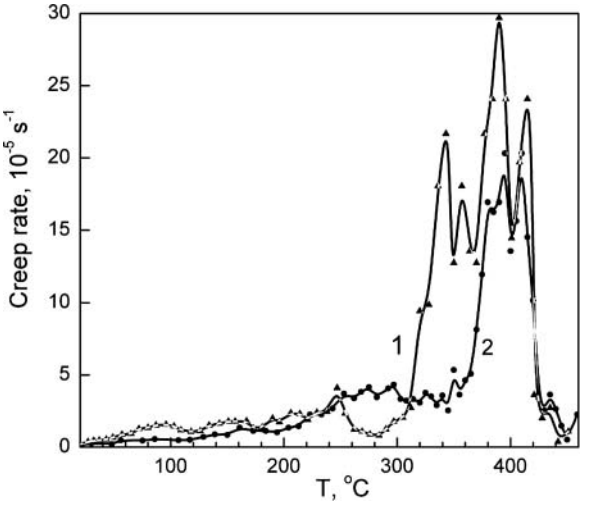

Figure 12. Creep rate spectra obtained at tensile stress 5 MPa for (1) neat PI-II and (2) PI-I/MWCNT-COOH (0.5 wt%).

Downloaded by [Harbin Institute of Technology] at 18:47 28 December 2013

dynamics effects and an enhanced creep resistance of the composite: decreasing creep rates at moderate temperatures, the suppression of peaks at 340°C and 360°C and decreasing doublet peak at 390°C–410°C were observed.

Figure 10b shows an ambiguous impact of MWCNT-COOH on the PI-II dynamic modulus E' as shown by DMA over the 20°C–400°C range: adding of 0.25 or 0.5 wt% nanotubes did not significantly change the E' values whereas introducing 0.125 or 1 wt% COOH-modified nanotubes slightly decreased this parameter. This result we relate to the low stresses (<1 MPa) in DMA experiments.

Stress-strain Testing of the PI-Based Nanocomposites

As follows from the mechanical testing data summarized in Table 1, introduction of nanotubes slightly affected the mechanical properties of PI-I at room temperature. In fact, adding of 0.5 wt% MWCNT-COOH caused a small rise of the Young's modulus E, yield stress σ_y, and the break stress σ_b values of the films. This effect was absent while using untreated MWCNTs (0.5 wt%). Increasing of the MWCNT-COOH concentration up to 1 wt% led to a fall of modulus down to a value that was practically equal to that of the unfilled PI-I film. Such an effect, reported previously for the other PI nanocomposites,[31–33] reflects the onset of the nanoparticles aggregation process within the polymer matrix.

A progressive depression of the nanocomposite ultimate elongation value, ε_b, at room temperature was registered with increasing nanotube concentration (Table 1): the increasing of MWCNT-COOH concentration from 0 to 1 wt% led to an approximately twofold ε_b decrease. Again, similar effects have been reported previously while studying the introduction of different types of nanoparticles (nanoclay, asbestos-like hydrosilicate nanotibes, carbon nanofibers, and nanocones/discs) into PI matrices.[34,35] This effect of some PI "embrittlement" should be taken into account in all cases of PI-based nanocomposite films because it makes their practical use more difficult. However, the ultimate deformation value remained substantially higher than the strain at which the yield point was attained (∼10%) for the composite films under study, even at 1 wt% MWCNT-COOH.

Introduction of MWCNTs into the PI-II matrix led to a more substantial changing of the mechanical properties of PI-II at room temperature. Table 2 shows increasing E, σ_y, and σ_b values in the nanocomposites at different nanofiller loadings. While using modified MWCNTs, this rise takes place already at $c = 0.25$ wt% but it is maximal, by ∼20%–35%, at $c = 0.5$ wt%. Lesser increasing of these mechanical parameters was observed if 1 wt% MWCNT-COOH was added. Similarly, a substantially smaller effect of enhancing mechanical charactristics at room temperature was registered if untreated MWCNTs were used.

Table 1
Mechanical properties of PI-I/MWCNT nanocomposites at room temperature

Sample	E, GPa	σ_y, MPa	σ_b, MPa	ε_b,%
PI-I	3.30 ± 0.09	140 ± 4	138 ± 3	27 ± 2
PI-I/MWCNT-COOH (0.25%)	3.35 ± 0.09	142 ± 3	141 ± 3	18 ± 2
PI-I/MWCNT (0.5%)	3.40 ± 0.09	144 ± 4	142 ± 4	17 ± 2
PI-I/MWCNT-COOH (0.5%)	3.61 ± 0.12	150 ± 4	148 ± 4	16 ± 2
PI-I/MWCNT-COOH (1%)	3.36 ± 0.08	—	135 ± 4	15 ± 1

Downloaded by [Harbin Institute of Technology] at 18:47 28 December 2013

Table 2
Mechanical properties of PI-II/MWCNT nanocomposites at room temperature

Sample	E, GPa	σ_y, MPa	σ_b, MPa	ε_b,%
PI-II	3.75 ± 0.13	164 ± 3	181 ± 3	35 ± 4
PI-II/MWCNT-COOH (0.25%)	4.19 ± 0.10	185 ± 4	202 ± 4	34 ± 4
PI-II/MWCNT (0.5%)	4.00 ± 0.03	187 ± 3	194 ± 3	27 ± 2
PI-II/MWCNT-COOH (0.5%)	4.65 ± 0.12	199 ± 4	241 ± 5	35 ± 4
PI-II/MWCNT (1%)	4.03 ± 0.03	188 ± 3	204 ± 4	36 ± 4
PI-II/MWCNT-COOH (1%)	4.15 ± 0.05	188 ± 3	212 ± 4	51 ± 3

Of significance, the introduction of MWCNTs into PI-II matrix in all concentrations under study did not practically decrease the ultimate deformation of the films (a small negative effect was observed only while using 0.5 wt% of nontreated MWCNTs). Moreover, if 1 wt% MWCNT-COOH was used, the substantial increase of ε_b, from 35% to 51%, was registered. This latter unexpected effect needs additional investigation to be properly interpreted.

Finally, it should be stressed that mechanical tests of the strip-like specimens cut in various directions from both PI-I and PI-II-based composite films with different nanotube loadings showed no anisotropy of the mechanical properties. It means that an isotropic distribution of nanotubes was provided by the procedure of film formation used in this work.

Conclusion

1. A comprehensive, combined study of two series of PI/MWCNT composites based on the amorphous and semicrystalline matrices, with or without fluorine atoms, with 0.125–1.0 wt% COOH-functionalized or pristine nanotubes was performed using seven experimental techniques. Structure, morphology, nanotube dispersion, high temperature dynamics, and mechanical properties of the nanocomposites were studied.
2. Introducing of the MWCNT-COOH into the amorphous PI matrix had a slight influence on its structure while more cardinal changes arose in the semicrystalline PI matrix. Different characters of nanotube dispersion were also observed depending not only on MWCNT functionalization but also on the matrix structure. Generally, the best quality of nanotube dispersion was observed in the composites with 0.5 wt% MWCNT-COOH, and the greatest aggregation occurred with the pristine nanotubes. However, a specific character of nanotube dispersion was observed in the semicrystalline matrix: besides individually separated and uniformly dispersed nanotubes, small aggregates were located within the intercrystalline layers of the matrix.
3. Different peculiarities of high temperature dynamics were found in the nanocomposites studied. These included such effects as the appearance of a second, new glass transition region associated with the peculiar interfacial dynamics and displaced by 80°C–130°C to higher temperatures; the strong suppression of dynamics within and below the main glass transition; enhanced dynamics by nanotubes, and manifestation of a pronounced dynamic heterogeneity in the glass transition.

Downloaded by [Harbin Institute of Technology] at 18:47 28 December 2013

4. It was assumed that the strongest impact on suppression of segmental dynamics and increasing creep resistance was caused by the synergistic influence of two types of rigid "constraints"—nanotubes and PI crystallites—and by the enhanced (covalent and hydrogen bonds) interfacial interactions between them and disordered regions of PI.
5. A substantial enhancement of mechanical properties at room temperature, without decreasing elongation at break, was attained after introducing 0.5 wt% MWCNT-COOH into the semicrystalline PI matrix.

Downloaded by [Harbin Institute of Technology] at 18:47 28 December 2013

Acknowledgments

The financial support from National Natural Science Foundation of China (No. 51010005, 90916020), the Program for New Century Excellent Talents in University of China (NCET-08-0168), and the Fundamental Research Funds for the Central Universities of China (HIT.ICRST.2010001) is acknowledged. The authors would like to thank Hongwei Zhou and Xiaogang Zhao from the Alan G. MacDiarmid Institute, Jilin University of China, for experimental assistance and valuable discussion.

References

1. Iijima, S. Helical microtubules of graphitic carbon. Nature **1991**, *354*, 56.
2. Spitalsky, Z.; Tasis, D.; Papagelis, D.; Galiotis, S. Carbon nantube-polymer composites: chemistry, processing, mechanical and electrical properties. Progr. Polym. Sci. **2010**, *35*, 357.
3. Sahoo, N.G.; Rana, S.; Cho, J.W.; Li, L.; Chan, S.H. Polymer nanocomposites based on functionalized carbon nanotubes. Progr. Polym. Sci. **2010**, *35*, 837.
4. Valenkov, A.M.; Gofman, I.V.; Nosov, K.S.; Shapovalov, V.M.; Yudin, V.E. Polymeric composite systems modified with allotropic forms of carbon (review). Russ. J. Appl. Chem. **2011**, *84*, 735.
5. Pagona, G.; Mountrichas, G.; Kotas, G.; Karousis, N.; Pispas, S.; Tarmatarchis, N. Properties, applications and functionalization of carbon nanotubes. Intern. J. Nanotechnol. **2009**, *6*, 176.
6. Wu, H.-C.; Chang, X.; Liu, L.; Zhao, F.; Zhao, Y. Chemistry of carbon nanotubes in biomedical applications. J. Mater. Chem. **2010**, *20*(6), 1036.
7. Bessonov, M.I.; Koton, M.M.; Kudryavtsev, V.V.; Laius, L.A. *Polyimides: A Class of Thermally Stable Polymer*; Leningrad: Nauka, **1983**.
8. *Polyimides: Fundamentals and Applications*; Ghosh, M.K., Mittal, K.L., Eds., Marcel Dekker: New York, 1996.
9. Zhu, B.-K.; Xie, S.-H.; Xu, Z.-K.; Xu, Y.-Y. Preparation and properties of the polyimide/ multi-walled carbon nanotube nanocomposites. Compos. Sci. Technol. **2006**, *66*, 548.
10. Yuen, S.-M.; Ma, C.-C.M.; Chiang, C.-L.; Lin, Y.-Y.; Teng, C.-C. Preparation and morphological, electrical, and mechanical properties of polyimide-grafted MWCNT/polyimide composite. J. Polym. Sci. Part A, Polym. Chem. **2007**, *45*, 3349.
11. Mo, T.-C.; Wang, H.-W.; Chen, S.-Y.; Yen, Y.-C. Synthesis and characterization of polyimide/multi-walled carbon nanotube nanocomposites. Polym. Compos. **2008**, *29*, 451.
12. Schlea, M.R.; Brown, T.R.; Bush, J.R.; Jim, M.; Criss, Jr., J.M.; Mintz, E.A.; Shofner, M.L. Dispersion control and characterization in multi-walled carbon nanotube and phenylethynyl-terminated imide composites. Compos. Sci. Technol. **2010**, *70*, 822.
13. Wu, K.-L.; Chou, S.-C.; Cheng. Y.-Y. Comparison of polyimide/multi-walled carbon nanotube nanocomposites by in situ polymerization and blending. J. Appl. Polym. Sci. **2010**; *116*(6): 3111.
14. Yuen, S.-M.; Ma, C.-C.M.; Lin, Y.Y.; Kuan, H.C. Preparation, morphology and properties of acid and amine modified multi-walled carbon nanotube/polyimide composites. Compos. Sci. Technol. **2007**, *67*, 2564.

15. Chou, W.-J.; Wang, C.-C.; Chen, C.-Y. Characteristics of polyimide-based nanocomposites containing plasma-modified multi-walled carbon nanotubes. Compos. Sci. Technol. **2008**, *68*, 2208.
16. Cai, H.; Yan, F.; Xue, Q. Investigation of tribological properties of polyimide/carbon nanotube nanocomposites. Mater. Sci. Eng. A **2004**, *364*, 94.
17. So, H.H.; Cho, J.W.; Sahoo, N.G. Effect of carbon nanotubes on mechanical and electrical properties of polyimide/carbon nanotube nanocomposites. Europ. Polym. J. **2007**, *43*, 3750.
18. Feiring, A.E.; Brian, J.; Awnan, C.; Wonchobat, E.R. Synthesis and properties of fluorinated polyimides from novel 2,2′-bis(fluoroalkoxy) benzidines. Macromolecules **1993**, *26*, 2779.
19. Li, F.; Fang, S.; Ge, J.J.; Honigfort, P.S.; Chen, J.C.; Harris, F.W.; Cheng, S.Z.D. Diamine architecture effects on glass transitions, relaxation processes and other material properties in organo-soluble aromatic polyimide films. Polymer **1999**, *40*, 4571.
20. Ounaies, Z.; Park, C.; Wise, K.E.; Siochi, E.J.; Harrison, J.S. Electrical properties of single wall carbon nanotube reinforced polyimide composites. Compos. Sci. Technol. **2003**, *63*, 1637.
21. Watson, K.A.; Donavon, S.G.; Delozier, M.; Smith, Jr., J.G.; Connell, J.W. Transparent, flexible, conductive carbon nanotube coatings for electrostatic charge mitigation. Polymer **2005**, *46*, 2076.
22. Bershtein, V.A.; Yakushev, P.N. Laser-interferometric creep rate spectroscopy of polymers. Adv. Polym. Sci. **2010**, *230*, 73.
23. De Fonton, S.; Oberlin, A.; Inagaki, M. Characterization by electron microscopy of carbon phases (intermediate turbostratic phase and graphite) in hard carbons when heat-treated under pressure. J. Mater. Sci. **1980**, *15*, 909.
24. Neki, K.; Geil, P.H. Morphology-properties studies of amorphous polycarbonate. J. Macromol. Sci.-Phys. **1974**, *8*, 295.
25. Hobbs, J.K.; Farrance, O.E.; Kailas, L. How atomic force microscopy has contributed to our understanding of polymer crystallization. Polymer **2009**, *50*, 4281.
26. Magonov, S.N.; Godovsky, Y.K. Visualization of granular nanostructure in crystalline polymers by AFM. Am. Lab. **1999**, *31*, 52.
27. Hugel, T.; Strobl, G.; Thomann, R. Building lamellae from blocks: the pathway followed in the formation of crystallites of syndiotactic polypropylene. Acta Polym. **1999**, *50*, 214.
28. Giannelis, E.P.; Krishnamoorti, R.; Manias, E. Polymer-silicate nanocomposites: model systems for confined polymers and polymer brushes. Adv. Polym. Sci. **1999**, *138*, 107.
29. Wunderlich, B. Reversible crystallization and the rigid amorphous phase in semi-crystalline polymers. Progr. Polym. Sci. **2003**, *28*, 383.
30. Bershtein, V.A.; Sukhanova, T.E.; Krizan, T.D.; Keating, M.Y.; Grigoriev, A.I.; Egorov, V.M.; Yakushev, P.N.; Peschanskaya, N.N.; Vylegzhanina, M.E.; Bursian, A.E. Relationship of processing conditions to structure and properties in PMDA-ODA polyimide. J. Macromol. Sci.-Phys. **2005**, *44*, 613.
31. Chang, J.-H.; Park, D.-K.; Ihn, K.J. Polyimide nanocomposite with a hexadecylamine clay: synthesis and characterization. J. Appl. Polym. Sci. **2002**, *84*, 2294.
32. Gofman, I.V.; Svetlichnyi, V.M.; Yudin, V.E.; Dobrodumov, A.V.; Didenko, A.L.; Abalov, I.V.; Korytkova, E.N.; Egorov, A.I.; Gusarov, V.V. Modification of films of heat-resistant polyimides by adding hydrosilicate and carbon nanoparticles of various geometries. Russ. J. Gen. Chem. **2007**, *77*, 1158.
33. Ray, S.S.; Bousmina, M. Biodegradable polymers and their layered silicate nanocomposites. Progr. Mater. Sci. **2005**, *50*, 962.
34. Delozier, D.M.; Orwoll, R.A.; Cahoon, J.F.; Johnston, N.J.; Smith, Jr., J.G.; Connell, J.W. Preparation and characterization of polyimide/organoclay nanocomposites. Polymer **2002**, *43*, 813.
35. Gofman, I.V.; Abalov, I.V.; Yudin, V.E.; Tiranov, V.G. Mechanical and thermal properties of nanocomposite films based on an aromatic polyimide and carbon nanocones. Solid State Phys. **2011**, *53*, 1509.

Downloaded by [Harbin Institute of Technology] at 18:47 28 December 2013